JOURNAL OF GEOPHYSICAL RESEARCH, VOL. 105, NO. B11, PAGES 25,391–25,402, NOVEMBER 10, 2000

Investigating the frequency dependence of mantle Q by stacking P and PP spectra

Linda M. Warren and Peter M. Shearer
Institute of Geophysics and Planetary Physics, Scripps Institution of Oceanography
University of California, San Diego

Abstract. Using seismograms from globally distributed, shallow earthquakes between 1988 and 1998, we compute spectra for P arrivals from epicentral distances of 40° to 80° and PP arrivals from 80° to 160°. Selecting records with estimated signal-to-noise ratios greater than 2, we find 17,836 P and 14,721 PP spectra. We correct each spectrum for the known instrument response and for an ω^{-2} source model that accounts for varying event sizes. Next, we stack the logarithms of the P and PP spectra in bins of similar source-receiver range. The stacked log spectra, denoted as $\log(D'_P)$ and $\log(D'_{PP})$, appear stable between about 0.16 and 0.86 Hz, with noise and/or bias affecting the results at higher frequencies. Assuming that source spectral differences are randomly distributed, then for shallow events, when the PP range is twice the P range, the average residual source spectrum may be estimated as $2\log(D'_P) - \log(D'_{PP})$, and the average P wave attenuation spectrum may be estimated as $\log(D'_{PP}) - \log(D'_P)$. The residual source spectral estimates exhibit a smooth additional falloff as $\omega^{-0.15\pm0.05}$ between 0.16 and 0.86 Hz, indicating that $\omega^{-2.15\pm0.05}$ is an appropriate average source model for shallow events. The attenuation spectra show little distance dependence over this band and have a P wave $\overline{t^*}$ value of ~0.5 s. We use $\overline{t^*}$ measurements from individual P and PP spectra to invert for a frequency-independent Q model and find that the upper mantle is nearly 5 times as attenuating as the lower mantle. Frequency dependence in Q_α is difficult to resolve directly in these data but, as previous researchers have noted, is required to reconcile these values with long-period Q estimates. Using Q model QL6 [*Durek and Ekström*, 1996] as a long-period constraint, we experiment with fitting our stacked log spectra with an absorption band model. We find that the upper corner frequency f_2 in the absorption band must be depth-dependent to account for the lack of a strong distance dependence in our observed $\overline{t^*}$ values. In particular, our results indicate that f_2 is higher in the top 220 km of the mantle than at greater depths; the lower layer is about twice as attenuating at 1 Hz than at 0.1 Hz, whereas the upper mantle attenuation is relatively constant across this band.

1. Introduction

As seismic waves propagate through the Earth, their amplitudes decay due to energy loss to anelastic and scattering processes. Many studies of anelastic attenuation at long periods, while perhaps recognizing the frequency dependence of the quality factor Q, have not been concerned with quantifying it over wide frequency bands. However, if the long-period Q values held for higher frequencies, the high-frequency energy would be dissipated to below the noise level at much lower frequencies than is seen [*Der et al.*, 1982b]. Thus a frequency dependence, with larger Q at higher frequencies, is required. This type of frequency dependence is consistent with thermally activated relaxation processes, which theoretical considerations suggest are responsible for the attenuation. The degree of attenuation at a given location will be determined not only by the temperature and pressure but also by the distribution of dislocation lengths and the stress state [*Lundquist and Cormier*, 1980].

While low-frequency studies measure attenuation from normal modes and surface waves, high-frequency studies measure the decay of body waves from waveform amplitudes and/or the shape of the spectral falloff. We will focus on the spectral methods for measuring the decay of P waves at relatively high frequencies (~0.15 to 1 Hz). The computed spectrum for a P wave, $D_P(f)$, is affected not only by the along-path attenuation, $A_P(f)$, but also by the source spectrum $S(f)$, the known in-

Paper number 2000JB900283.
0148-0227/00/2000JB900283$09.00

strument response $R(f)$, and the geometrical spreading term G:

$$D_P(f) = A_P(f)\, S(f)\, R(f)\, /G. \quad (1)$$

While the instrument response is known for all stations and can be removed, there is less certainty in the source spectral falloff at higher frequencies. The most common models suggest that above the corner frequency, the average source spectrum falls off as ω^{-n}, where n is between 2 and 3 [e.g., *Mueller and Murphy*, 1971; *Helmberger and Hadley*, 1981]. This range in n values leads to a nonuniqueness in the determination of the effects caused by path attenuation as opposed to the source spectrum.

Many high-frequency studies have been confined to specific geographic regions or paths, such as parts of the United States [e.g., *Der et al.*, 1982a; *Der and Lees*, 1985], the Eurasian shield [e.g., *Der et al.*, 1986], back arc basins [e.g., *Barazangi et al.*, 1975; *Flanagan and Wiens*, 1998], and paths from central Asian test sites or the northwest Pacific subduction zones to seismic arrays [e.g., *Bache et al.*, 1985, 1986; *Sharrock et al.*, 1995a, b; *Walck*, 1988]. These studies have demonstrated that there are large variations in Q in the upper mantle, often related to the tectonic history of the area. For example, low Q values are typically found under back arc basins, mid-ocean ridges, and tectonically active regions, while high Q zones are generally found under old oceanic crust and continental shields.

Rather than focusing on a specific region, we are interested in the globally averaged attenuation structure of the mantle as can be measured using the large data sets available from the global seismic networks. We stack the logarithms of thousands of P and PP spectra to distinguish between the source and attenuation components of the spectra and then apply these results to find the globally averaged Q values for the upper and lower mantles at frequencies of 0.16 to 0.86 Hz. We also present a frequency- and depth-dependent absorption band model to jointly interpret these measurements with long-period results from previous studies.

2. Data and Processing

We select our seismograms from the Incorporated Research Institutions for Seismology (IRIS) Fast Archive Recovery Method (FARM) database [*Ahern et al.*, 1995] for 1988 to 1998, which includes all earthquakes during this time with $M_W \geq 5.8$ (with $M_W \geq 5.5$ for quakes at $\geq$100 km depth). While the original database is composed of 20 Hz data, we have applied an antialiasing filter and resampled at 5 Hz for a local database that is used for a variety of seismic studies. We search the local database for all P arrivals at epicentral distances between 40° and 80° and all PP arrivals between 80° and 160° from shallow ($\leq$50 km depth) earthquakes. Next, after applying a Hanning taper we compute the spectrum for a 12.6-s-long signal window beginning 2 s before each predicted arrival time and for a 12.6-s-long noise window just preceding this. An example seismogram with its spectrum is shown in Figure 1. In the ensuing analysis we select spectra that have average signal-to-noise ratios of 2 or greater between 0.16 and 0.86 Hz. This results in 17,836 P and 14,721 PP spectra from 1553 events and 151 stations. Signal-to-noise ratios of 3 and 5 give similar results in our analyses below; we choose the lower cutoff to include a more global distribution of data and to not exclude more attenuating paths. The upper limit on the frequency band is determined by noise in the PP spectra; by ~1 Hz most PP spectra have been attenuated to below the noise level.

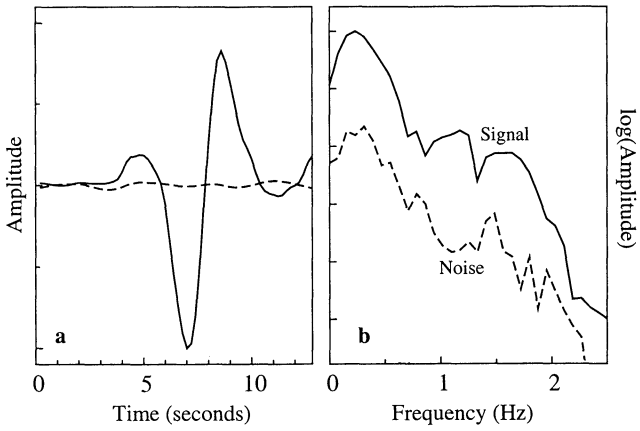

Figure 1. (a) A seismogram recorded at station HIA on January 22, 1988, from a 5-km-deep earthquake 70° away and (b) its spectrum. In the spectral plot, each tick on the log-amplitude axis represents an order of magnitude. The solid line is the signal, while the dashed line is the noise. The noise window ends 2 s before the signal window begins. For this example, the spectral signal-to-noise ratio is 38.

Each computed spectrum represents the effects of the source, propagation, and instrument responses. Because we are interested in the along-path effects, we correct for the known instrument responses (including our antialiasing filter) and a source model. We approximate the source with a falloff of ω^{-2} above the corner frequency and a corner frequency ω_c that depends on moment magnitude M_0. The moment rate spectral density is given by [e.g., *Houston and Kanamori*, 1986]

$$\hat{M}(\omega) = \frac{M_0\, \omega_c^2}{\omega_c^2 + \omega^2} \quad (2)$$

with

$$\frac{\omega_c}{2\pi} = 0.49\, \beta \left[\frac{\Delta\sigma}{M_0}\right]^{\frac{1}{3}}, \quad (3)$$

where $\beta = 3.75$ km/s is the S wave velocity and $\Delta\sigma =$ 30 bars is the assumed stress drop. After making these corrections for the instrument response and source spectrum the remaining spectrum, denoted as D'_P and D'_{PP}

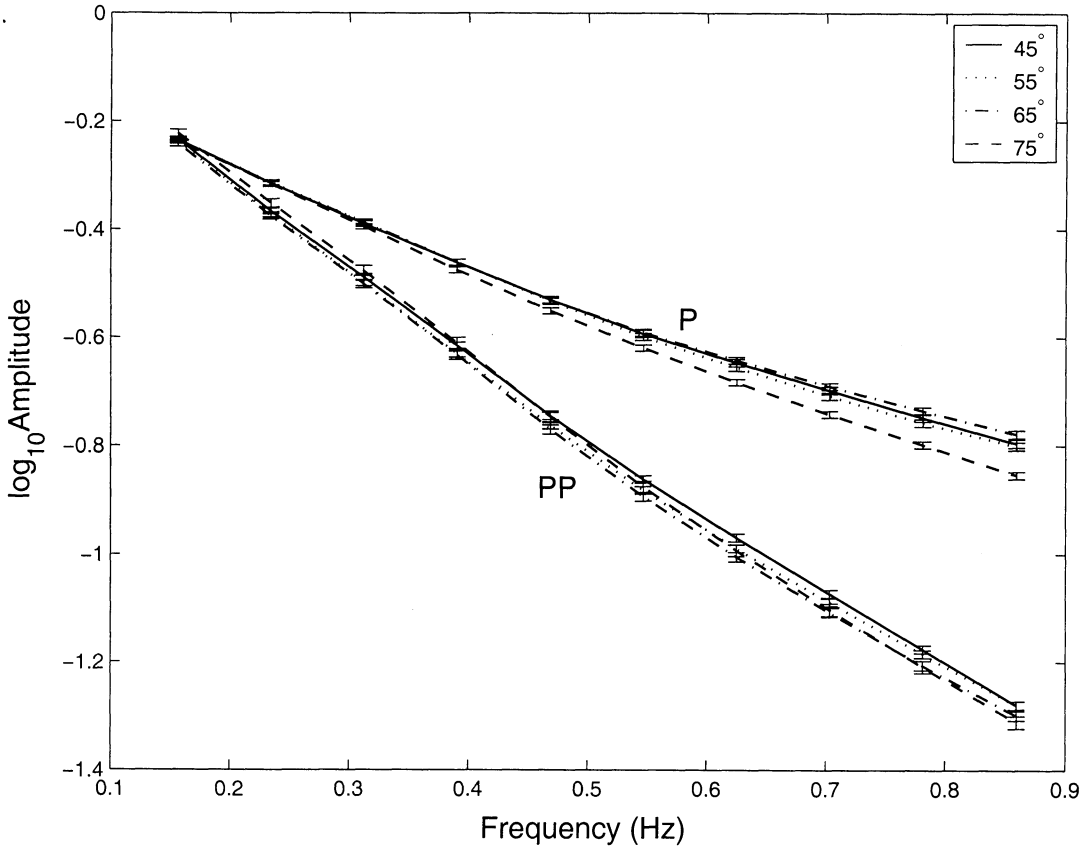

Figure 2. Stacks of the P and PP log spectra. The stacked PP log spectra are more attenuated (have less high-frequency energy) than the stacked P log spectra. The estimated standard errors are indicated by the error bars. For both phases, there is little distance dependence. For ease in comparison of relative slopes all stacks are aligned to the same amplitude at 0.16 Hz.

for the P and PP spectra, respectively, should result from along-path attenuation. Because each individual spectrum is affected by random fluctuations, we stack them to find a smooth spectrum describing the average propagation response. The stacking method simply sums the logarithms of the individual spectra and normalizes the amplitude of the resulting stack to a reference frequency. In this way, the shape of the spectrum from a small event will have equal impact on the stack as the spectrum from a large event. Our analyses throughout this paper are concerned only with the relative shape of the spectra, not their absolute amplitudes.

We compute stacks for the P wave log spectra in range bins of 40°–50°, 50°–60°, 60°–70°, and 70°–80° and the PP wave log spectra in range bins of 80°–100°, 100°–120°, 120°–140°, and 140°–160°. Henceforth we will refer to these range bins by their midpoint values of 45°, 55°, 65°, and 75° for the stacked P log spectra. The stacked PP log spectra bins will be referred to with the same numbers, representing half their midpoint ranges. The stacked log spectra for these range bins are shown in Figure 2. The standard errors, which were estimated from bootstrap resampling [*Efron*, 1982], are also included. As expected, the stacked PP log spectra are approximately twice as attenuated as the stacked P log spectra. For both phases the relative slopes for the different range bins show that there is only slightly more attenuation at the largest distances.

3. Separation of Source and Attenuation Components of the Spectrum

Our stacked logarithmic spectra provide PP arrivals at twice the distance of the P arrivals. While the stacked P and PP log spectra contain the same residual source component, if any remains, the stacked PP log spectra should be twice as attenuated as the stacked P log spectra since the PP waves travel twice as far as the P waves. We separate the average residual source and attenuation components of the spectrum by taking different combinations of the P and PP spectra. We compute these combinations using the stacked PP log spectra at twice the distance of the stacked P log spectra, giving us four estimates of these quantities corresponding to the four different distance bins. Note that we do not analyze P and PP on individual seismograms since we require that the PP source-receiver range be

double the P range. Rather, our technique is applied to the stacks of thousands of traces which we assume approximate the globally averaged P and PP attenuation.

The observed P and PP spectra, after correcting for the known instrument response and an ω^{-2} source model (corrected observed and source spectra denoted by prime) and substituting $A(f) = A^0 e^{-\pi f t_P^*}$ for the amplitude decay with frequency into (1), are

$$D'_P(f) = A_P^0 e^{-\pi f t_P^*} S'(f)/G \quad (4a)$$

$$D'_{PP}(f) = A_{PP}^0 e^{-\pi f 2t_P^*} S'(f) C/G^2 \quad (4b)$$

for PP at twice the range of P, where the P and PP subscripts are for the P and PP spectra, C is the reflection coefficient at the PP bounce point, G is the geometrical spreading term, and t_P^* is the average t^* for a P wave. The quantity $t^* = \int dt/Q$ is the integrated travel time scaled by $1/Q$ along the ray path. Taking the base 10 logarithm of (4) gives

$$\log(D'_P) = \log(A_P^0) - 0.4343\,\pi\, f\, t_P^* + \log(S') - \log(G) \quad (5a)$$

$$\log(D'_{PP}) = \log(A_{PP}^0) - 2 \times 0.4343\,\pi\, f\, t_P^* + \log(S') - 2\log(G) + \log(C). \quad (5b)$$

These two equations have two frequency-dependent unknowns, the average attenuation response and the residual source spectrum, which we can solve for.

Attenuation, which is quantified by t^*, can be isolated by subtracting the stacked P log spectrum from the stacked PP log spectrum:

$$\log(D'_{PP}) - \log(D'_P) = \log(A_{PP}^0) - \log(A_P^0) - 0.4343\,\pi f t_P^* - \log(G) + \log(C). \quad (6)$$

Since A_P^0, A_{PP}^0, C, and G are constant with frequency, they will change the amplitude of the curve but not its slope. The average attenuation spectrum only depends upon the frequency-dependent portion of this difference so we set the constant terms to zero. Thus the attenuation component of the spectrum is

$$-0.4343\,\pi\, f\, t_P^*(f) = \log[D'_{PP}(f)] - \log[D'_P(f)]. \quad (7)$$

A cartoon illustrating this equation is shown in Figure 3a, while the differential spectrum for each range bin is plotted in Figure 3b. From (7) it appears that t^* can be measured directly from the differential spectrum. However, as we will see later, t^* changes too quickly with frequency over the frequency band that we are investigating to measure attenuation by simply fit-

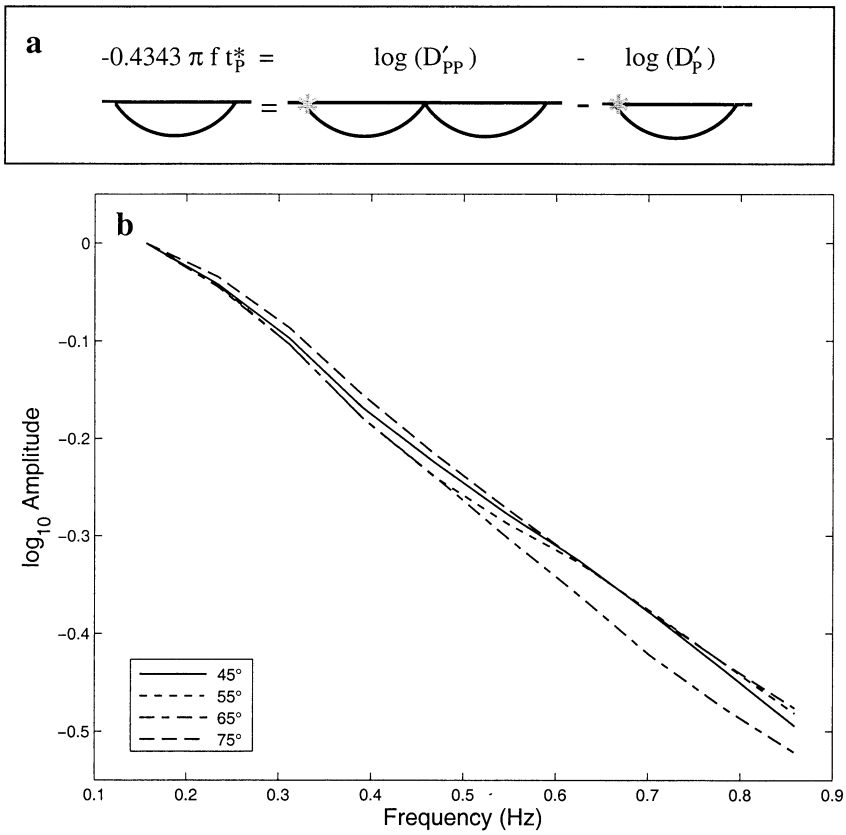

Figure 3. The average attenuation spectrum for a P wave. We isolate the average attenuation spectrum for a P wave by computing the difference $\log(D'_{PP}) - \log(D'_P)$. (a) Cartoon demonstrating what this difference represents and (b) computed difference for the range bins of our stacked log spectra. We find $\overline{t^*} = 0.53$ s. Again the stacks are aligned at 0.16 Hz.

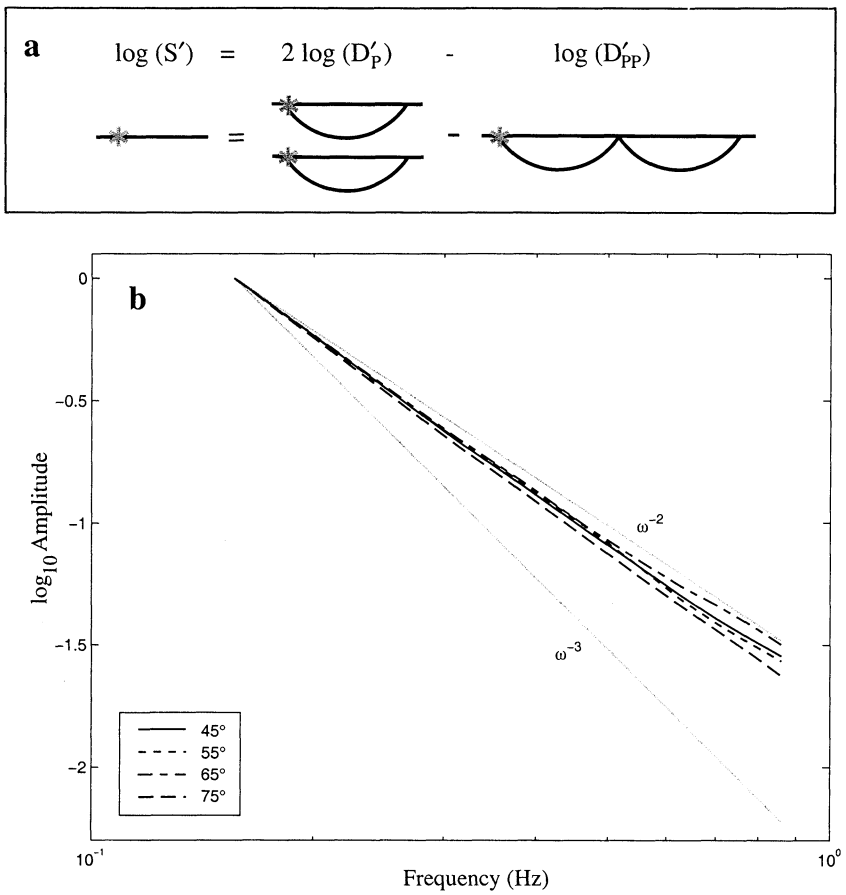

Figure 4. The average residual source spectrum. After correcting for an ω^{-2} source model we extract the residual source spectrum by computing the differential log spectrum $2\log(D'_P) - \log(D'_{PP})$. (a) Cartoon demonstrating what this difference represents and (b) computed difference for the range bins of our stacked log spectra. For the differential spectrum we have added ω^{-2} back in so that comparisons with ω^{-2} and ω^{-3} models can be made easily. The average observed source spectrum has an $\omega^{-2.15}$ falloff.

ting a straight line to the differential log spectrum. The quantity actually measured by fitting a straight line to the log spectrum is known as the apparent t^*, or $\overline{t^*}$. It is defined as

$$\overline{t^*} = -\frac{d(\ln A)}{\pi\, df} = t^* + f\frac{dt^*}{df}. \tag{8}$$

Fitting a line to the differential attenuation spectrum gives an average value of $\overline{t^*} = 0.53$ s for all range bins.

We can isolate the residual source spectrum, $S'(f)$, by subtracting the stacked PP log spectrum from twice the stacked P log spectrum:

$$2\log(D'_P) - \log(D'_{PP}) = 2\log(A^0_P) - \log(A^0_{PP}) + \log(S') - \log(C). \tag{9}$$

Again, A^0_P, A^0_{PP}, and C are constant and will not change the slope of the curve, so the residual source spectrum, after setting the constant terms to zero, is given by

$$\log[S'(f)] = 2\log[D'_P(f)] - \log[D'_{PP}(f)] \tag{10}$$

A cartoon illustrating this equation is shown in Figure 4a, while the differential spectrum for each range bin (with ω^{-2} added back in for comparison purposes) is plotted in Figure 4b. In principle, details of the average source spectrum that have not been removed by the ω^{-2} model of (2) will appear in the differential spectra. In particular, if a different ω exponent were more appropriate, then the residual source spectra should plot in Figure 4b as straight lines with a different slope than ω^{-2}. Fits to the residual source spectra at frequencies between 0.16 and 0.86 give slopes of –0.1 to –0.2, suggesting that an $\omega^{-2.15}$ source model would provide a better fit to our data. To avoid projecting the residual source spectral slope into our attenuation measurements, we correct our data for an $\omega^{-2.15}$ model in subsequent analyses. However, note that the most significant deviations from the ω^{-2} slope occur between 0.16 and 0.3 Hz, a band that spans the range of typical corner frequencies in our source model (which, from (3), decrease from 0.31 Hz for $M_W = 5.8$ to 0.16 Hz for $M_W = 6.4$). Thus it is possible that inaccuracies in our

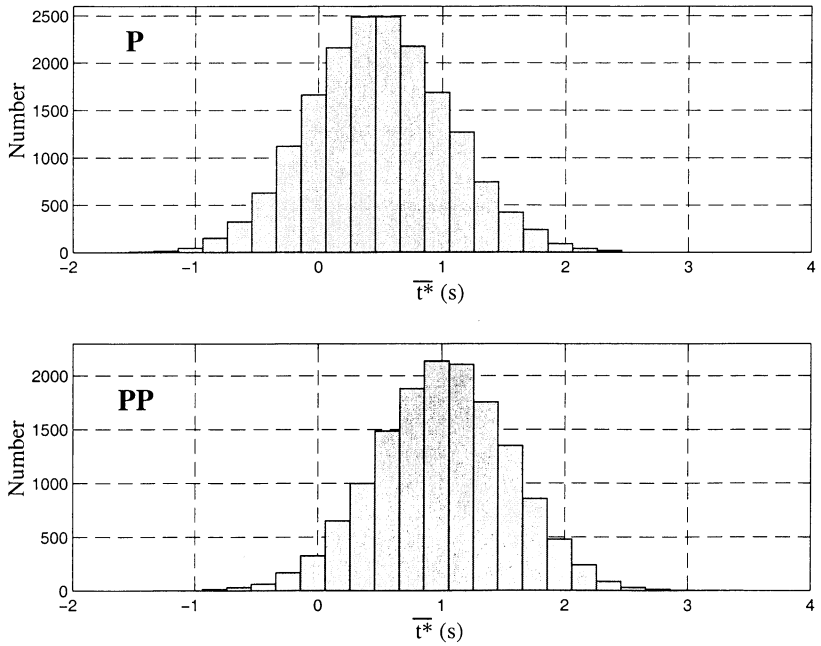

Figure 5. Histograms of the P and PP $\overline{t^*}$ measurements. There are 17,836 P and 14,721 PP spectra. The PP values are roughly double the P values, indicating that the PP arrivals are twice as attenuated as the P arrivals.

corner frequency estimates are biasing our results over this band and causing the misfit to the ω^{-2} model. In any case, the measured deviations from the ω^{-2} model are fairly small; our results favor average source models with spectral falloffs between ω^{-2} and $\omega^{-2.2}$ over the 0.16 and 0.86 Hz band, while models with ω exponents of –2.5 or –3 would severely misfit our data.

4. One-Dimensional, Frequency-Independent Q Model

Although, in general, Q is a frequency-dependent quantity, it is often approximated as independent of frequency over a limited frequency range, in which case $dt^*/df = 0$ and $\overline{t^*} = t^*$. In this section, we adopt this approach and invert our $\overline{t^*}$ measurements directly for a two-layer Q_α model. It should be emphasized, however, that this model is only valid for predicting observed $\overline{t^*}$ values across the frequency band of our observations. As we discuss in section 5, the likely frequency dependence of Q at these frequencies means that the Q_α values are overestimated. We obtain $\overline{t^*}$ from the individual P and PP log spectra that we have computed. We measure the average slope of each log spectrum using least squares to fit a straight line between 0.16 and 0.86 Hz. Histograms of these measurements are shown in Figure 5. The mean values are $\overline{t^*}_P = 0.48$ s and $\overline{t^*}_{PP} = 0.97$ s. Measurements for all distance ranges are grouped together because there is only minor distance dependence (see Figure 6): For the P waves, there is a $\overline{t^*}$ increase of 0.0017 s/deg, while for the PP waves the increase is 0.0011 s/deg. Both of these measurements translate to increases of <0.1 s from the smallest to the largest distances covered in this study.

We combine the 32,557 $\overline{t^*}$ measurements from the P and PP spectra with travel times from the IASPEI 1991 velocity model [*Kennett*, 1991] to invert for a two-layer, globally averaged Q model. In separate inversions we

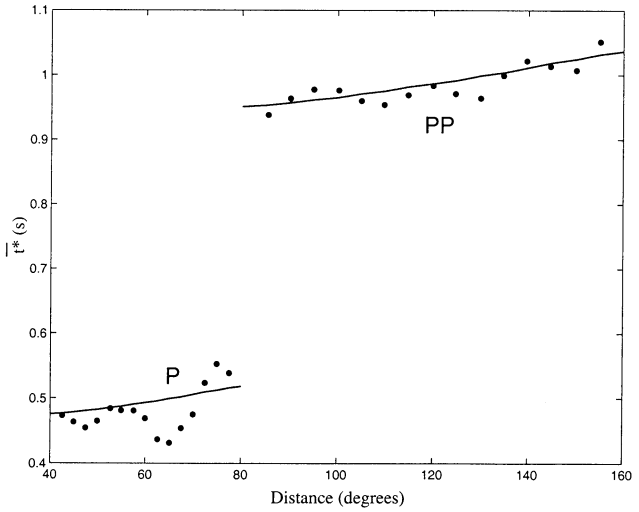

Figure 6. The distance dependence of $\overline{t^*}$. The $\overline{t^*}(\Delta)$ predictions of our frequency-independent Q model with the 660-km-thick upper layer (solid lines) are compared with our mean measured $\overline{t^*}$ values (dots). The P wave $\overline{t^*}$ measurements are averaged in overlapping bins 5° wide spaced by 2.5°. The PP wave $\overline{t^*}$ measurements are averaged in 10° bins spaced by 5°. The median values give similar results.

Table 1. Two-Layer Frequency-Independent Model

Boundary	This Study		QL6	
Depth, km	Q_{UL}	Q_{LL}	Q_{UL}	Q_{LL}
220	185	3250	170	595
410	335	3005	215	655
660	535	2595	245	800

fix the boundary depth between the two layers at 220, 410, and 660 km depth, traditional boundary depths in the upper mantle. The resulting least squares Q values (denoted Q_{UL} for the upper layer and Q_{LL} for the lower layer) are shown in Table 1 and compared with long-period results, which will be discussed later. For our three models the top layer is much more attenuating than the bottom layer. There is a trade-off between upper layer thickness and Q values; thinner layers have smaller Q values, while thicker layers have larger Q values. All models give nearly identical fits to the data, and in Figure 6 the distance dependence predicted by the 660-km-thick upper layer model is compared with that observed in the $\overline{t^*}$ measurements. Our predictions agree well with the overall trend of the measurements.

Because of the ray geometry we do not have the resolution to solve for more than a single layer for the upper mantle or to distinguish which boundary depth best represents the Earth. It is unlikely that attenuation in the upper mantle is uniform; our value for Q_{UL}^{-1} represents an average of Q^{-1} over the entire upper layer. Using bootstrap resampling [*Efron*, 1982], we estimate the standard errors in Q^{-1} for the model with the 660-km-thick upper layer to be $\pm 1.7\%$ in the upper mantle and $\pm 3.5\%$ in the lower mantle. The estimated errors are quite small because of our large data set. A much larger source of uncertainty in the model is the effect of neglecting the frequency dependence of attenuation across the 0.16 to 0.86 Hz band. As we will show in section 5, much lower Q values than those of this simple frequency-independent model are required when the frequency dependence is taken into account.

5. Absorption Band Modeling

Our results by themselves do not span a wide enough frequency band to directly resolve any frequency dependence in Q. However, as noted in previous studies [e.g., *Sipkin and Jordan*, 1979; *Lundquist and Cormier*, 1980; *Anderson and Given*, 1982; *Der et al.*, 1986], the clearest evidence for frequency-dependent attenuation comes from comparisons between Q studies at long periods (20–100 s) and those at high frequencies ($\sim$1 Hz). Thus we experiment with fitting both our stacked log spectra and the long-period constraints provided by other studies with an absorption band model. The frequency dependence of the quality factor, as described by an absorption band with relaxation times continuously distributed between τ_1 and τ_2 (at the low- and high-frequency ends, respectively), is

$$Q^{-1}(\omega) = Q_m^{-1}\left(\frac{2}{\pi}\tan^{-1}\left[\frac{\omega(\tau_1-\tau_2)}{1+\omega^2\tau_1\tau_2}\right]\right) \qquad (11)$$

where $\omega = 2\pi f$ and the minimum Q value (maximum attenuation) is given by Q_m [*Lundquist and Cormier*, 1980]. Within the absorption band, attenuation is nearly independent of frequency f, while at higher frequencies, Q is proportional to f and at lower frequencies it is proportional to $1/f$. Since the composition and properties of the mantle change with temperature, pressure, and depth, the location of the absorption band also may change. With increasing temperature the band will shift to higher frequencies, while with increasing pressure it will shift to lower frequencies. The band will also shift to lower frequencies with a decrease in stress. Thus, with increasing depth the band would be expected to shift to lower frequencies because pressure generally dominates over temperature in the upper mantle and because tectonic stress decreases [*Anderson and Given*, 1982].

Since we expect the location of the absorption band to change with depth and we have already seen differences in Q with depth in the frequency-independent model, we model the mantle with two independent absorption band layers. We experiment with different high-frequency relaxation times (τ_2), low-frequency Q_m values, and boundary depths between the layers. Since we are interested in the frequency dependence at the high-frequency end of the absorption band, the long-period relaxation time, as long as it is slow enough, does not matter, and we use $\tau_1 = 10^4$ s/rad. For each model we calculate $t^*(f)$, compute the log spectrum for the frequencies of our stacked log spectra, and measure $\overline{t^*}(f)$ from the log spectrum. We compare the model predictions for $\overline{t^*}(f)$ with "instantaneous" $\overline{t^*}(f)$ measurements made for each neighboring pair of frequency points in the stacked P and PP log spectra. The advantage to using instantaneous $\overline{t^*}$ measurements rather than a single measurement over a large frequency band is that it allows us to see small changes in $\overline{t^*}$ with frequency. If attenuation were constant with frequency, the $\overline{t^*}$ measurements would also be constant and equal to t^*.

We can fit our data with little frequency dependence in the upper layer but require significant frequency dependence in the lower layer. Using Q model QL6 [*Durek and Ekström*, 1996] as a low-frequency constraint for Q_α values and applying an absorption band with upper corner frequency $f_2 = 1/(2\pi\tau_2) = 2.5$ Hz in the upper 220 km of the mantle and $f_2 = 0.8$ Hz at greater depths, we can fit our observations fairly well. The $\overline{t^*}(f)$ predictions of this model are compared with our instantaneous $\overline{t^*}$ measurements in Figure 7a. The measured $\overline{t^*}$ values decrease slowly with frequency over

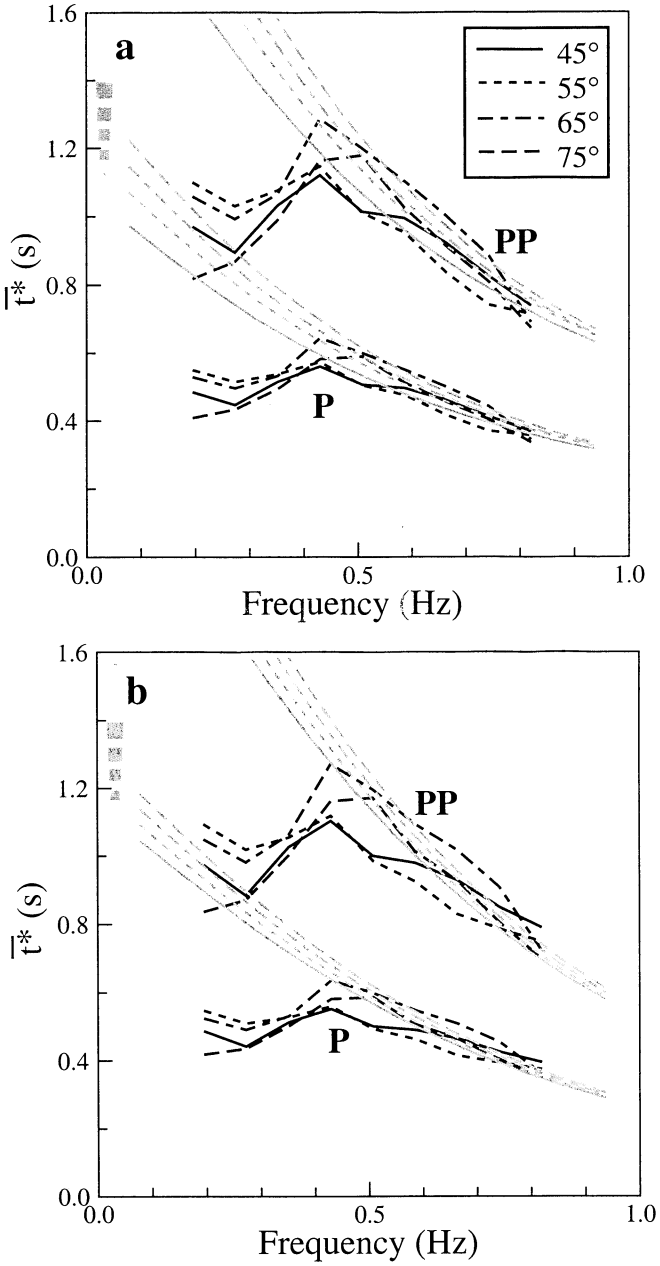

Figure 7. A comparison between our observations (solid lines) and our predictions from a two-layer absorption band model (shaded lines) for P and PP $\overline{t^*}$ values. Predictions for models with the layer break at (a) 220 km and (b) 660 km depth and f_2 values given in the text are shown. The squares on the left side are the P wave t^* predictions of QL6 [*Durek and Ekström*, 1996], which provide the long-period constraints for the absorption band. The top square is for a distance of 75°. Since the absorption band is relatively flat at the low frequencies of QL6, the t^* values should not differ significantly from the $\overline{t^*}$ values.

the frequency band that we have measured and are significantly smaller than the long-period results (the squares on the left side of Figure 7). It was not possible to fit our stacked log spectra perfectly with the absorption band model while also satisfying the long-period constraint on Q. In particular, the increase in $\overline{t^*}$ values seen between 0.2 and 0.45 Hz cannot easily be explained by any simple frequency-dependent Q model. Our preferred model overpredicts observed $\overline{t^*}$ values over this band but does achieve a reasonable overall fit to $\overline{t^*}$ as a function of time and distance, especially between 0.45 and 0.8 Hz. The Q values for this model as a function of frequency are shown in Table 2. Note that the Q_{UL} values do not increase significantly until frequencies above 1 Hz. In contrast, Q_{LL} more than doubles between 10 and 1 s. The lower mantle in our model is ~3 times less attenuating than the upper mantle at 100 s and 6 times less attenuating at 1 s.

If we fit an absorption band model with a thicker layer in the upper mantle, we require a stronger frequency dependence in the upper mantle ($f_2 = 1.25$ Hz for 660-km boundary) while the upper corner frequency in the lower mantle remains fairly constant ($f_2 = 0.95$ Hz for 660-km boundary). For a 660-km-thick upper layer the predicted $\overline{t^*}$ values fall off somewhat more steeply with frequency than our measured values (see Figure 7b).

6. Discussion

It has been known for some time that the upper mantle is more attenuating to seismic waves than the lower mantle [e.g., *Anderson and Hart*, 1978]. Our results show that this difference becomes more pronounced at higher frequencies. Because the paths through the upper mantle are of similar lengths for all distance ranges while those through the lower mantle are much more variable in length, the similar slopes of the stacks for the different range bins and the small measured $\overline{t^*}$ increase with distance suggest that Q is much smaller in the upper mantle than in the lower mantle. The frequency-independent inversion for Q_α, where we find that the average Q in the lower mantle is >4 times larger than it is in the upper mantle, confirms this. Comparing our Q values directly with low-frequency Q values averaged over the same depths (see Table 1) reveals better agreement in the upper mantle than in the lower mantle, again suggesting that the frequency dependence in the lower mantle is stronger than in the upper mantle. In Table 1 we show $1/\overline{Q^{-1}}$ for Q model QL6 [*Durek and Ekström*, 1996]. While QL6 has four layers in the

Table 2. Two-Layer Mantle Absorption Band Model

Period, s	Frequency, Hz	Q_{UL}	Q_{LL}
1000	0.001	174	601
100	0.01	173	599
10	0.1	177	645
1	1	227	1383
0.1	10	1103	11,688

Mantle above 220 km depth $Q_m = 170$, $f_2 = 2.5$ Hz and mantle below 220 km depth $Q_m = 595$, $f_2 = 0.8$ Hz

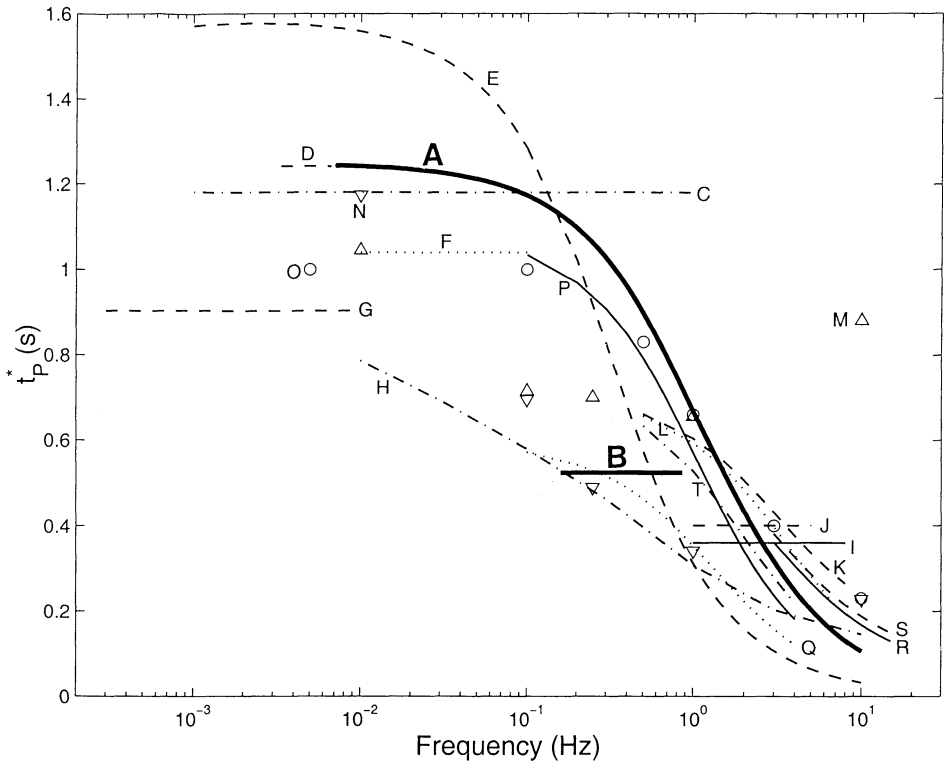

Figure 8. A comparison of P wave $t^*(f)$ predictions of various models. The two models we have described in this paper (heavy lines) are compared with previous results. The models are plotted at the frequency or over the range of frequencies specified in the study. Those models that have a distance dependence are plotted for an epicentral distance of 55°. For many of the studies the distance dependence is small. Some of the studies, particularly the long-period ones, have been converted to P wave attenuation from shear attenuation or shear and bulk attenuation (Q_μ and Q_κ, respectively) measurements using $Q_\alpha^{-1} = LQ_\mu^{-1} + (1-L)\,Q_\kappa^{-1}$, where $L = \frac{4}{3}(\beta/\alpha)^2 = 4/9$ for a Poisson solid. If Q_κ was not specified, it was assumed to be infinite, a reasonable assumption since most of the attenuation occurs in shear [*Anderson and Given*, 1982]. Models A and B are the absorption band and frequency-independent models presented in this study. The other models shown are PREM of *Dziewonski and Anderson* [1981] (C, dash-dotted); QL6 of *Durek and Ekström* [1996] (D, dashed); *Sipkin and Jordan* [1979] (E, dashed); SL8 of *Anderson and Hart* [1978] (F, dotted); *Widmer et al.* [1991] (G, dashed); EURS of *Der et al.* [1986] (H, dash-dotted); *Sharrock et al.* [1995a] (I, solid); *Archambeau et al.* [1969] (J, dashed); *Bache et al.* [1986] (K, dashed, and L, dotted, for paths to arrays of the United Kingdom Atomic Energy Authority and to NORSAR); *Anderson and Given* [1982] (M, triangles, and N, inverted triangles, for t_P^* and $t_S^*/4$ predictions); *Lundquist and Cormier* [1980] (O, circles); *Der et al.*[1982b] (P, solid, and Q, dotted, for shield-tectonic and shield-shield paths); *Walck* [1988] (R, solid, and S, dashed, for paths from the Soviet Degelan and Shagan River test sites to NORESS); and *Der et al.* [1982a] (T, dash-dotted).

mantle, we have computed $\overline{Q^{-1}}$ from these layers for the two layers of our models.

When we fit an absorption band model to the stacked log spectra, we find that the upper corner frequency (f_2) in the lower mantle is lower than the corresponding frequency in the upper mantle and the absorption band is centered at lower frequencies. Since the position of the absorption band is related to, among other properties, the pressure, temperature, and stress, this shift in location of the absorption band is consistent with the expected shift to lower frequencies with depth due to decreasing tectonic stress and increasing pressure [*Anderson and Given*, 1982]. The different locations for the absorption band result in Q_{UL} being relatively constant between 1000 and 1 s period, while Q_{LL} increases eightfold over this band.

The frequency dependence of P wave t^* predicted by our two models at a distance of 55° is compared with the predictions of other studies in Figure 8. The frequency-independent model is plotted for the frequency range we have measured $\overline{t^*}$ (0.16 to 0.86 Hz), while the absorption band model is constrained at lower frequencies by previous long-period results and extrapolated to higher frequencies. Most of the previous models are restricted to either high or low frequencies. In comparing the models we should also note that while the low-frequency studies

tend to be global models, the high-frequency ones are generally restricted to certain regions, such as Eurasia or the southwestern United States, or types of regions, such as shields or tectonically active zones.

First, looking at our frequency-independent model, which is restricted to relatively high frequencies, we see that its predictions lie just above those for shield models [e.g., *Der et al.*, 1982b, 1986]. Since shields are among the least attenuating regions, our global model should predict larger t^* values than those found from the shield models; we would expect values closer to those for tectonic regions and mixed tectonic-shield paths. Our predicted t^* values only match the mixed tectonic-shield path values at the highest frequencies that we measure, and at lower frequencies we underestimate t^*. The underprediction that we see can be explained by the assumption we make in determining the frequency-independent model that the change in t^* with frequency is negligible. While this assumption means that $\overline{t^*}$ and t^* are equal, the absorption band model has shown that t^* decreases with increasing frequency (i.e., $dt^*/df < 0$). If we could account for the frequency-dependent term in (8), it would increase the predicted t^* values. Figure 9 compares the sizes of $t^*(f)$ for our absorption band model with the resulting $\overline{t^*}(f)$ values and frequency-dependent term from (8). At 0.5 Hz, the midpoint of our frequency range, t^* is 0.29 s larger than $\overline{t^*}$.

Since the absorption band model accounts for a frequency dependence in t^*, it should better predict the true values of t^*. Our absorption band model generally agrees with the previous high-frequency absorption band models. Many of the high-frequency studies also fit absorption bands to spectra, although they typically use a single absorption band. This is more appropriate for their data than ours because those studies are often for specific paths at relatively short distances, so the waves mostly travel through the upper mantle. Our model is different from most high-frequency studies in that we have also fit low-frequency constraints. The low-frequency studies have much scatter in their predicted t^* values due to the different types of data and measurement methods. We have used QL6 [*Durek and Ekström*, 1996] as our long-period constraint.

Other studies that have combined high- and low-frequency data to look at the frequency dependence of attenuation show varied results. Model EURS [*Der et al.*, 1986] is restricted to the Eurasian shield, so we will simply note that its predicted t^* values fall below ours, as would be expected. *Anderson and Given* [1982] fit an absorption band to body wave, surface wave, and normal mode data. They fix Q_m (minimum Q or maximum attenuation) and the width of the absorption band but allow the location of the band to change with depth. Similar to our results, they require markedly different locations for the absorption band in the upper and lower mantles, with the band centered at longer periods in the lower mantle. They also see a distinct layer at the base of the mantle where the absorption band shifts back to higher frequencies, as in the upper mantle. The range of our data does not allow us to resolve this feature, if it exists. The t_P^* predictions of Anderson and Given, after initially decreasing, actually increase from 1 to 10 Hz and are significantly larger than observations at 10 Hz. If their t_S^* predictions are scaled by a factor of 1/4, which is equivalent to having all energy loss be from shear deformation [*Der et al.*, 1986], the

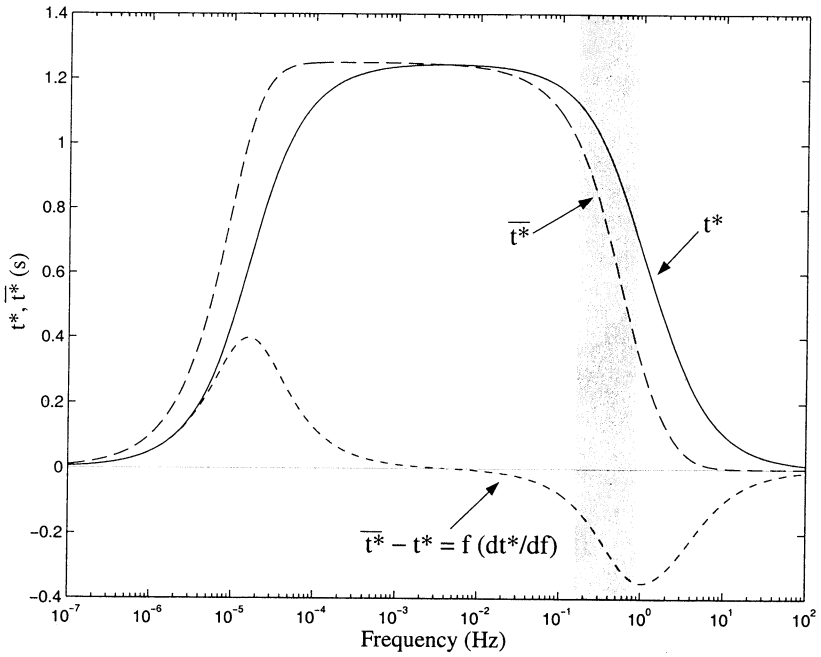

Figure 9. A comparison of $t^*(f)$ and $\overline{t^*}(f)$ for our absorption band model. For the frequencies of our stacks (shaded area), t^* is larger than $\overline{t^*}$ by 0.1–0.3 s.

$t^*(f)$ curve continuously decreases with increasing frequency, although the falloff begins at lower frequencies than other studies.

Sipkin and Jordan [1979] have combined data from a number of different frequency bands to put upper and lower limits on an absorption band model. They limit f_2 to between 0.2 and 1 Hz, and Figure 8 shows the curve for a middle value of $f_2 = 0.5$ Hz. Since they fit a single absorption band to the whole mantle, their predicted t^* values are strongly distance-dependent and, at 55° (the distance for which the models are plotted), are too large at low frequencies. Their range of predicted t^* values at higher frequencies, while consistent with other models, tends to have a steeper falloff with frequency than most. This could reflect their data being confined to a specific region (the western Pacific) rather than being global in distribution.

The preferred model of *Lundquist and Cormier*[1980] has a double absorption band. They superimpose an absorption band with constant parameters ($Q_m = 120$ and $\tau_2 = 0.005$ s/rad) for depths of 45 to 200 km on a whole mantle absorption band that has τ_2 increasing exponentially with depth from about 0.09 s/rad at the top of the mantle to ~0.7 s/rad at the base of the mantle. At low frequencies their model, which converges to SL8 [*Anderson and Hart*, 1978], underestimates t^*, while across the middle- to high-frequency band their predictions agree well with other studies. This model is quite similar to ours in that they also find that they better fit the data with separate absorption bands for the upper and lower mantles and that the upper mantle has a shorter relaxation time than the lower mantle. Their average relaxation times for the upper and lower mantles are similar to ours. Similar results were also found by *Choy and Cormier* [1986] for the attenuation of S and ScS waves in the mantle. They find low Q in the upper mantle (to a depth of 400 km) for frequencies of 0.01 to 5 Hz. The intensity of Q at depths of 400 to 2000 km varies with frequency; Q is high for $f \gg 0.3$ Hz, while Q is low for $f \ll 0.3$ Hz.

Comparisons among studies show that some properties of attenuation in the mantle, such as the existence of depth and frequency dependencies, are well established. However, the detailed forms of theses properties are not well resolved. While some of the discrepancy at specific frequencies is due to differences in methods and data types used, much of it is caused by variations in the regional coverage of the data sampling. In this paper we have presented an average global model for the depth and frequency dependence of Q_α in the mantle. Future work will involve using the retrieved spectra to map lateral variability in the attenuation.

Acknowledgments. We thank Paul Earle and Luciana Astiz for help obtaining the FARM data and IRIS for providing and maintaining the database. This work was supported by an NSF Graduate Research Fellowship and NSF grant EAR96-14350.

References

Ahern, T., R. Benson, and K. Creager, New FARM products, yours for the picking, *IRIS Newsl., 14,* 14-15, 1995.

Anderson, D. L., and J. W. Given, Absorption band Q model for the Earth, *J. Geophys. Res., 87,* 3893-3904, 1982.

Anderson, D. L., and R. S. Hart, Q of the Earth, *J. Geophys. Res., 83,* 5869-5882, 1978.

Archambeau, C. B., E. A. Flinn, and D. G. Lambert, Fine structure of the upper mantle, *J. Geophys. Res., 74,* 5825-5865, 1969.

Bache, T. C., P. D. Marshall, and L. B. Bache, Q for teleseismic P waves from central Asia, *J. Geophys. Res., 90,* 3575-3587, 1985.

Bache, T. C., S. R. Bratt, and H. Bungum, High-frequency P wave attenuation along five teleseismic paths from central Asia, *Geophys. J. R. Astron. Soc., 85,* 505-522, 1986.

Barazangi, M., W. Pennington, and B. Isacks Global study of seismic wave attenuation in the upper mantle behind island arcs using pP waves, *J. Geophys. Res., 80,* 1079-1092, 1975.

Choy, G. L., and V. F. Cormier Direct measurement of the mantle attenuation operator from broadband P and S waveforms, *J. Geophys. Res., 91,* 7326-7342, 1986.

Der, Z. A., and A. C. Lees, Methodologies for estimating $t^*(f)$ from short-period body waves and regional variations of $t^*(f)$ in the United States, *Geophys. J. R. Astron. Soc., 82,* 125-140, 1985.

Der, Z.A., T.W. McElfresh, and A. O'Donnell, An investigation of the regional variations and frequency dependence of anelastic attenuation in the mantle under the United States in the 0.5–4 Hz band, *Geophys. J. R. Astron. Soc., 69,* 67-99, 1982a.

Der, Z.A., W.D. Rivers, T.W. McElfresh, A. O'Donnell, P.J. Klouda, and M.E. Marshall, Worldwide variations in the attenuative properties of the upper mantle as determined from spectral studies of short-period body waves, *Phys. Earth Planet. Inter., 30,* 12-25, 1982b.

Der, Z. A., A. C. Lees, and V. F. Cormier, Frequency dependence of Q in the mantle underlying the shield areas of Eurasia, part III, the Q model, *Geophys. J. R. Astron. Soc., 87,* 1103-1112, 1986.

Durek, J. J., and G. Ekström, A radial model of anelasticity consistent with long-period surface-wave attenuation, *Bull. Seismol. Soc. Am., 86,* 144-158, 1996.

Dziewonski, A. M., and D. L. Anderson, Preliminary reference Earth model (PREM), *Phys. Earth Planet. Inter., 25,* 297-365, 1981.

Efron, B. *The Jackknife, the Bootstrap and Other Resampling Plans, CBMS-NSF Reg. Conf. Ser. Appl. Math.,* vol 38, Soc for Ind. and Appl. Math., Philadephia, Pa, 1982.

Flanagan, M. P., and D. A. Wiens, Attenuation of broadband P and S waves in Tonga: Observations of frequency dependent Q, *Pure Appl. Geophys.,153,* 345-375, 1998.

Helmberger, D. V., and D. M. Hadley, Seismic source functions and attenuation from local and teleseismic observations of the NTS events JORUM and HANDLEY, *Bull. Seismol. Soc. Am., 71,* 51-67, 1981.

Houston, H., and H. Kanamori, Source spectra of great earthquakes: Teleseismic constraints on rupture process and strong motion, *Bull. Seismol. Soc. Am., 76,* 19-42, 1986.

Kennett, B. L. N., *IASPEI 1991 Seismological Tables,* Res. Sch. of Earth Sci., Aust. Nat. Univ., Canaberra, ACT, 1991.

Lundquist, G. M., and V. F. Cormier, Constraints on the

absorption band model of Q, *J. Geophys. Res., 85,* 5244-5256, 1980.

Mueller, R. A. and J. R. Murphy, Seismic characteristics of underground nuclear detonations, *Bull. Seismol. Soc. Am., 61,* 1675-1692, 1971.

Sharrock, D. S., I. G. Main, and A. Douglas, A two-layer attenuation model for the upper mantle at short periods, *Geophys. Res. Lett., 22,* 2561-2564, 1995a.

Sharrock, D. S., I. G. Main, and A. Douglas, Observations of Q from the Northwest Pacific subduction zone recorded at teleseismic distances, *Bull. Seismol. Soc. Am., 85,* 237-253, 1995b.

Sipkin, S. A., and T. H. Jordan, Frequency dependence of Q_{ScS}, *Bull. Seismol. Soc. Am., 69,* 1055-1079, 1979.

Walck, M. C., Spectral estimates of teleseismic P wave attenuation to 15 Hz, *Bull. Seismol. Soc. Am., 78,* 726-740, 1988.

Widmer, R., G. Masters, and F. Gilbert, Spherically symmetric attenuation within the Earth from normal mode data, *Geophys. J. Int.,96,* 541-553, 1991.

P. M. Shearer and L. M. Warren, IGPP, Scripps Institution of Oceanography, University of California, San Diego, La Jolla, CA 92093-0225. (lwarren@ucsd.edu)

(Received February 14, 2000; revised June 23, 2000; accepted July 21, 2000.)